

CONF-961119-1

SAND96-2232C

SAND--96-2232C

Atomic-Scale Dynamics of Atoms and Dimers on the Si(001) Surface

B. S. Swartzentruber

Sandia National Laboratories, Albuquerque, NM 87185-1413

The kinetics of adsorbed Si monomers and dimers, at submonolayer coverage, are measured using scanning tunneling microscopy (STM). Si monomers are observed in empty-state STM images acquired between room temperature and 115 C. The monomers are trapped at the ends of rebonded-SB type dimer rows. When monomers thermally escape from the traps, they rapidly diffuse along the substrate dimer row until they find another unoccupied trap or return to their original trap. The binding activation barrier at isolated traps is ~ 1.0 eV. A slightly lower barrier exists for monomers to hop between the ends of neighboring dimer rows – a process facilitating diffusion along segments of SB type steps. In addition to monomers, the interactions of adsorbed Si dimers with steps and islands on Si(001) are quantified using atom-tracking STM. Diffusing dimers are reflected from steps, sides of islands, and certain surface defect structures. Site-specific free energies are extracted from measurements of lattice-site occupation probabilities of dimers trapped between these reflecting barriers. Relative to the free energy of isolated dimers on a terrace, dimers located at the first lattice site next to SA steps and the sides of islands are bound by ~ 0.03 – 0.06 eV. The binding decreases to half that at the second lattice site, and is indistinguishable from the free-terrace value at a distance of three or more lattice sites.

keywords: Scanning tunneling microscopy, Diffusion and migration, Surface diffusion, Silicon, Surface defects, Clusters

DISTRIBUTION OF THIS DOCUMENT IS UNLIMITED

B. S. Swartzentruber

Sandia National Laboratories, Albuquerque, NM 87185-1413

phone: (505) 844-6393 fax: (505) 844-5470

email: bsswart@sandia.gov

MASTER

The growth of epitaxial thin films and overlayers occurs through the incorporation of deposited atoms into substrate crystal lattice positions either at steps or islands. The details of the growth morphology depend on the interplay between a number of surface kinetic processes that determine the rate at which atoms ultimately become incorporated into the lattice. These processes are governed by the thermodynamic stability, or binding free energy, of various configurations, and may depend in atomic-scale detail on a number of factors, such as: (1) diffusional anisotropy, (2) atomic sticking coefficients at steps, kinks, and islands, as well as with other atoms to form small clusters, (3) energetics of atom-defect interactions, and (4) substrate-potential variations that alter diffusion near possible binding sites. If small clusters are mobile on the surface, then their kinetic behavior must also be considered. A thorough understanding of the overall growth process thus requires a knowledge of atom and mobile-cluster kinetic processes and of how these processes compete to determine growth morphologies.

This work reports the investigation of two of the atomic-scale kinetic processes involved in homoepitaxial growth on the Si(001) surface. First, the atomic-scale behavior of the binding of silicon monomers at steps and islands on the Si(001) surface is measured directly using variable-temperature scanning tunneling microscopy (STM). And second, the Si dimer-substrate binding free energy as a function of location is extracted from measurements of the position and hop statistics of dimers as they migrate over the Si(001) surface in the thermodynamic limit.

The Si(001) surface reconstructs to form rows of dimerized atoms. Due to the crystal lattice structure, the bond direction on alternating layers is orthogonal which leads to two generally different types of steps. The edges of overlayer islands terminate with monatomic-height steps. As shown schematically in Fig. 1, step segments that are perpendicular to the lower-terrace dimer rows are called SA and those that are parallel to the lower-terrace dimer rows are called SB [1]. Furthermore, the SB steps can terminate in one of two locations with respect to the substrate dimer rows, ending either at the trough between the dimer rows (so-called non-bonded SB) or on top of the dimer rows (so-called rebonded SB). In the latter case, the edge atoms of the step rebond with those in the last row of the lower terrace. The

DISCLAIMER

This report was prepared as an account of work sponsored by an agency of the United States Government. Neither the United States Government nor any agency thereof, nor any of their employees, make any warranty, express or implied, or assumes any legal liability or responsibility for the accuracy, completeness, or usefulness of any information, apparatus, product, or process disclosed, or represents that its use would not infringe privately owned rights. Reference herein to any specific commercial product, process, or service by trade name, trademark, manufacturer, or otherwise does not necessarily constitute or imply its endorsement, recommendation, or favoring by the United States Government or any agency thereof. The views and opinions of authors expressed herein do not necessarily state or reflect those of the United States Government or any agency thereof.

DISCLAIMER

**Portions of this document may be illegible
in electronic image products. Images are
produced from the best available original
document.**

rebonded dimer bonds are depicted as gray in Fig. 1. The rebonded step configuration is energetically favored over the non-bonded step configuration [1].

For the case of homoepitaxial growth on Si(001), experiments pioneered by Mo and coworkers [2-5] investigated the anisotropic diffusion of Si atoms [2], the nucleation and growth of islands [3], and certain aspects of Si atom sticking at SA and SB steps [2,4]. In those studies, room temperature STM measurements of island shapes and distributions quenched during homoepitaxial growth on Si(001) were compared with Monte Carlo simulations to estimate values for the anisotropic diffusion of Si monomers and the anisotropic sticking of monomers at the SA and SB steps [2-5]. Other workers have investigated the energetics of steps [6-8], the kinetics of step-atom rearrangement [9-12], and the diffusion [13,14] and stability [15-17] of adsorbed Si dimers. Recent low-temperature STM measurements on substrates cold enough to freeze out monomer diffusion have observed the stable monomer adsorption site on the terrace [18,19]. In addition to the experimental work, there have been many recent theoretical investigations of adsorbed Si atom and dimer binding and diffusion using both first-principles and empirical-potential methods [20]. In particular, the first theoretical study to accurately predict the stable monomer-terrace adsorption site was performed by Brocks, Kelly, and Car using first-principles methods [21]. Several theoretical investigations have studied the interaction of monomers with steps using both first-principles [22-24] and empirical-potential [25-27] methods. All of these calculations find that monomers are effectively non-interacting with SA steps but bind to SB steps in agreement with Mo's experimental results. However, the *ab initio* results predict that the monomers bind very strongly to the rebonded SB steps while they do not interact with the non-bonded SB steps. In direct contrast, results using empirical potentials predict that monomers bind to the non-bonded SB steps and are not interacting with the rebonded SB steps. As shown below, this dramatic contradiction is resolved through direct observation of the preferred monomer binding sites at steps. In addition, the monomer-step binding energy is obtained from measurements of the monomer dynamics performed at elevated temperature.

The experiments are performed in an ultrahigh-vacuum scanning tunneling microscope (STM) with a base pressure of 5×10^{-11} torr. The samples are cleaned by annealing to 1250 C for several seconds [28]. To evaporate silicon atoms onto the clean substrate surface, a nearby

silicon wafer is heated to ~ 1150 C and an intervening shutter is opened for 10 s, resulting in the deposition of several percent of a monolayer of silicon atoms. The substrate temperature during evaporation is ~ 100 C. The samples are then transferred *in situ* to the variable-temperature STM where the temperature is set by resistive heating [11].

The contrast obtained in STM images of semiconductor surfaces is typically highly bias dependent, where the surface electronic-structure contrast may dominate over topographic contrast, *i.e.*, that which would be expected from the atomic coordinates [29]. This is most evident in the comparison of images acquired using filled (occupied) and empty (unoccupied) states. Fig. 2 shows filled and empty-state images of two regions of the Si(001) surface after the deposition of several percent of a monolayer of silicon. The pairs of images were acquired simultaneously at room temperature – the filled states, (a) and (c), while scanning left to right and the empty states, (b) and (d), while scanning right to left.

Differences in the spatial contrast between the two images are clearly evident. One of the most notable is the apparent contrast on the substrate dimer rows which appear as stripes in the images. In the filled-state images, Figs. 2(a) and (c), the bright stripes on the substrate correspond to the tops of the dimer rows, whereas, in the empty-state images, Figs. 2(b) and (d), the bright stripes correspond to the regions between the dimer rows [30]. Because the empty-state contrast is more sensitive to the dangling bonds, it is also much easier to see the structure associated with the individual atoms comprising clusters in the empty-state images. A short one-dimer-wide island appears as two narrow bands in the empty state image and as one thicker stripe in the filled-state image (seen, for example, in the upper right corner of Figs. 2(a) and (b)). However, within the scope of this work, the most important distinction between the filled and empty-state images is that unpaired monomers at island and step edges can be clearly imaged using empty states and are practically invisible using filled states. This is dramatically illustrated in the empty-state image of Fig. 2(d) in which monomers can be observed at the step edge. Historically, virtually all of the STM work on this surface measuring step and growth morphologies was performed using filled-state imaging, for the contrast in these images is more intuitively associated with the atomic structure. This may explain why information regarding the configuration and kinetics of monomer-containing structures has been lacking despite the vast amount of work on this system. The structural

information contained in the empty-state images is now only beginning to be exploited both experimentally [16,17] and theoretically [31].

When imaged at room temperature or above, after deposition at 100 C, unpaired monomers are found predominantly in one type of location that acts as a trap site. The monomers are bound only to the ends of SB-type dimer rows that have the rebonded termination. This observation directly confirms the predictions of the *ab initio* calculations [22-24], and contradicts those expected from the empirical-potential methods [25-27]. In this study, a monomer isolated on a terrace away from steps, islands, or clusters has never been observed. During the deposition process each monomer is able to find a stable binding site and/or the diffusion of an isolated monomer, even at room temperature, is so fast that it cannot be stably imaged and therefore remains unnoticed.

As easily determined from the images, trapped monomers are bound along the line of symmetry through the middle of the overlayer island dimer row; however, because of the strong electronic structure contribution to the image contrast, the exact position of the monomer along this line cannot be rigorously determined from the STM images. The *ab initio* calculations find the stable binding site at the so-called M position [23,24]. The two monomers shown in Fig. 1 are bound to the ends of rebonded dimer rows at this position. Incidentally, monomers can also bind to the ends of the metastable diluted-dimer row structures [16,31]; however, these structures will not be discussed here.

The monomers can escape from their traps at elevated temperature. Once a monomer escapes, it very rapidly diffuses in a random walk along the substrate dimer row to which it was originally bound until it finds another unoccupied trap terminating on that row or it returns to the initial trap. The two monomers depicted in Fig. 1 are shown in trap sites terminating on the same dimer row. Certain defects in the substrate row and SA-type steps terminating across the row act as reflection barriers that effectively confine the monomers to one-dimensional segments of the surface. Because the rate of monomer diffusion is extremely high compared to the rate at which the monomers escape from the traps, the monomers are only imaged in the trap sites. In fact, in the STM images, the only monomers that are *observed* to vacate the trap sites are those that can exchange between two or more trap sites along a single substrate row. The monomers that have only a single trap accessible to them

are always observed at the trap because upon leaving the trap they return on a time scale much more rapid than the imaging time scale.

Fig. 3 shows monomers exchanging between trap sites in two pairs of sequential empty-state images acquired at 105 C. The two pairs of traps are separated by 11 and 3 lattice sites in Figs. 3(a) and (b), respectively. Each trap is a rebonded-SB type end of an island dimer row. Every pair of traps terminates on a single substrate dimer row, the top of which shows up as a dark band in these empty-state images. The fact that the monomers are stable in these configurations of traps for many minutes is testament to the enormous diffusional anisotropy of silicon monomers on the Si(001) surface, for if the monomers make even one hop across the channel to a neighboring row they are lost to the local system. Additional evidence for the difficulty of a cross-channel hop is indicated by the fact that two traps terminating on neighboring substrate dimer rows have never been observed to share a monomer. Therefore, even the local strain associated with the step rebonding does not induce the monomer to cross the channel. However, the monomers can freely cross over the top of the dimer row and bind to traps on the opposite side, as seen in Fig. 3. Pairs of traps in which a monomer binds on opposite sides of the substrate dimer row and those in which a monomer binds on the same side of the row exist with equal likelihood.

The rate at which a monomer escapes from a trap is determined by the binding activation barrier. The STM data show the number of times that a monomer is observed to switch traps during the acquisition of a series of images. The number of observed switches is a measure of the number of times that a monomer leaves one trap and successfully random walks to the other without returning to the initial trap. From the average residence time of the monomers in the trap sites at 105 C, and assuming an attempt frequency of between 10^{12} and 10^{13} Hz [14], the estimated binding activation barrier of the traps is $\sim 1.0 \pm 0.1$ eV.

There is a significant systematic difference between the rate that monomers escape from isolated traps, *i.e.*, traps located at least several lattice sites from other islands or steps, and the rate that monomers switch between nearest-neighbor trap sites. In the process of switching between nearest-neighbor trap sites the monomer interacts only with rebonded type substrate dimers – the gray dimer bonds in Fig. 1. Fig. 4(a) shows two images of a pair of traps that are comprised of nearest-neighbor dimer rows. Here, two images are selected that

show the monomer mostly in the trap site at the end of each dimer row. The residence times at such nearest-neighbor traps are systematically at least an order of magnitude shorter than at isolated traps, indicating a lower barrier for trap binding of at least 100 meV. Although some nearest-neighbor trap sites are found at islands, they appear commonly as straight segments of the SB type steps. Fig. 4(b) shows such a step configuration in which the ends of 4 neighboring dimer rows terminate on the same lower-terrace dimer row. Recall that dimer rows appear as dark stripes in the empty-state images. These 4 trap sites share a single monomer which is shown located at the two end sites in the two images. Again, monomers in this type of configuration switch sites significantly faster than those located at isolated traps. The barrier lowering at straight segments of the SB steps facilitates edge diffusion along the step which in turn increases the rate that monomers find each other at the step during growth. The large density of reactive trap sites at the steps implies that during growth, and at temperatures where thermal fluctuations occur, the relative occupation of monomers at the steps is rather high. It is unknown how the presence of these monomers affects the edge and kink energetics.

When deposited onto a substrate at 100 C, most of the Si atoms become incorporated in small islands [3]. A small percentage of the atoms combine with one other to form stable adsorbed dimers that sit on top of the substrate dimer rows [15-17]. Unlike monomers, these dimers do not diffuse at room temperature. However, as temperature is increased they begin to hop between neighboring lattice sites on top of the dimer rows. Previous measurements of the dimer diffusion yielded an activation barrier of 0.94 eV [14]. This means that at 110 C, for example, the hop rate is on average 2-3 times per second. The dimers were shown to be reflected by certain vacancy-type defects that act as hard-wall repulsive barriers. Because the diffusion is so highly anisotropic, (*i.e.*, similar to monomers, migration occurs only parallel to the substrate dimer rows), dimers can become confined in a 1-d box, the walls of which consist of two repulsive barriers existing on a single dimer row.

Measurements of the dimer dynamics are performed using atom-tracking STM [14]. Conventional STM images are acquired in a 2-d raster, scanning line-by-line to build up an image. The rate at which dynamic events can be resolved is determined by the 2-d image acquisition time. In atom-tracking mode, the STM probe tip is locked onto a selected dimer

using two-dimensional lateral feedback. Once locked, the feedback electronics maintain the tip over the dimer as it diffuses over the substrate tracking its coordinates. The feedback maintains a lateral position of zero local slope — the top of the dimer is tracked by continually "climbing uphill". When a diffusion event occurs, the atom tracker quickly relocates to the dimer's new position. The atom-track data consist of the X, Y and Z feedback coordinates as a function of time. In the atom-tracker mode, the STM spends all of its time measuring the kinetics of the selected dimer. Thus, using atom tracking, the time response of the STM is increased by more than a factor of 1000 over conventional imaging modes.

Because the probe tip is continually maintained over the diffusing dimer while atom tracking, it is possible that the presence of the probe may alter the surface dynamics. In the work reported here, all of the measurements were acquired with tunneling parameters that are believed not to affect significantly the diffusion statistics [14]. Furthermore, in detailed measurements of the rotation kinetics of Si dimers as a function of applied field, it was shown that although the activation barriers can be slightly altered by the electric field, the relative configurational binding free energies are unaffected by the field [17].

Fig. 5 is a ~ 125 Å, filled-state STM image acquired at 110 C. Two terraces are shown, separated by an SA step. Two dimers are trapped between the SA step and vacancy-type defects. The SA step and the defects are repulsive barriers that constrain each dimer to diffuse within a 1-d potential well on the surface. The dimer at the top of the image has 4 lattice sites over which it can migrate; while, the dimer near the bottom of the image can migrate among 6 lattice sites. Each dimer random walks in its well, with statistics governed by the local substrate potential.

Fig. 6 is a time-line plot of the atom-track diffusion data for the dimer at the top of Fig. 5, that is, the distance of the dimer from the step in the direction along the substrate dimer row versus time. Because the time response of the atom-tracker feedback is much faster than the average residence time, *i.e.*, the time between hops, the probability of missing a diffusion event in which the dimer hops over and back between sites faster than the feedback can respond is very small. *When every diffusion event can be captured, the statistics of the diffusion process can be analyzed directly*, without the assumptions implicit in a classical

random-walk analysis. This is in contrast to FIM measurements where atoms are allowed to diffuse for finite time intervals, after which snapshots of the atom position are acquired [33].

Two measurements are extracted from the atom-track data: the rate at which the dimer hops from each site, and the relative dimer occupation probability at each site. The first is determined by the local activation barriers, and the latter is governed by the local binding free energies. Because the activation barrier is the difference between the free energy of the transition state and the binding free energy at the stable sites, the hopping rate and the occupation probability are intrinsically linked through detailed balance. The difference in the activation barrier between two neighboring sites is equal to the difference in the binding free energy of the two sites.

A cursory look at Fig. 6 reveals that the occupation probability falls off as a function of the distance from the step. The dimer spends much more time in site #1, right next to the step, than in site #4, next to the vacancy-type defect. Similarly, the rate at which the dimer leaves a site increases away from the step. This is shown quantitatively in the residence time distribution data plotted in Fig. 7. These data are acquired from several data sets, such as that in Fig. 6, and contain a total of 354 hops over 330 seconds. The complete residence-time distribution for all 4 sites is plotted in Fig. 7(a) as open circles. In a random-walk process where the hopping probability, governed by the activation barrier, is the same throughout the diffusion interval, the residence-time distribution has the form of an exponential decay with a time constant equal to the average residence time. The dashed line is a plot of this “random walk” form with a decay time equal to the measured average residence time. The large deviation between the dashed line and the measured data is certainly not surprising, given the site-to-site variation in the activation barrier evident in the time-line plot. This variation is seen quite clearly when the residence-time distributions are plotted for each of the 4 sites independently (Fig. 7(b)). The data for each site show a characteristic decay time determined by the effective activation barrier at that site. The complete data set is very well described by a sum of exponentials, one for each site, with decay constants equal to the measured average residence times at each site, and weighted by the number of visits to each site. The weighted sum is displayed as the solid line in Fig. 7(a).

As mentioned above, the dimer occupation probabilities yield the relative binding free energies. The site-dependent binding free energies for both the dimer confined in the narrow well (4 sites, at the top of Fig. 5) and the dimer confined to the wider well (6 sites, at the bottom of Fig. 5) are plotted in Fig. 8 as a function of distance from the SA step. For these data sets, the error in the extracted free energy due to counting statistics is about ± 0.004 eV, which is smaller than the symbol size in Fig. 8. Since the measurement gives only the *relative* free energies, the free energy values for each data set are shown relative to the site directly next to the step. The lowest free energy in both data sets is right next to the step, and the highest free energy exists at the site next to the vacancy-type defect. It was shown in earlier work [14] that the free energy of an dimer next to certain vacancy-type defects is higher than that for an isolated dimer on the terrace by ~ 0.025 – 0.030 eV. Furthermore, the dimer–defect interaction was observed to be effective only at the site directly next to the defect, *i.e.*, at a distance of 1 lattice site. At separations of 2 or more, the free energy was constant — the free-terrace value.

Here, the free energy of the dimer in the narrow well continually increases between the step and the defect; whereas, the free energy in the slightly wider well levels off before increasing again at the defect. These plots reveal an dimer–step interaction falling off over a range of several sites away from the step. A well containing 6 sites may be wide enough that those in the middle are effectively free-terrace sites.

For comparison with these rather narrow wells, measurements are shown below for several wider ones, the walls of which are made up of various types of reflecting defects. Figs. 9(a)–(c) show empty-state images of 3 such wells containing 10, 12, and 14 sites respectively. The walls in these structures are comprised of: (a), the SA side of a Si island on the left, and one of the pair of coupled dimers on the right; (b), the SA side of an island on the left, and the upper edge of an SB step on the right; and (c), an unknown, Si-containing defect on the left, and a vacancy-type defect on the right. The free-energy plots for each of these wells are shown in Fig. 9(d) as open symbols. Additionally, the free-energy plot from Fig. 8 of the well with 6 sites is plotted with crosses. Since the position of the dimer in each well is measured relative to the left wall, the positions of the right walls are located at varying distances on this plot.

Each of the three wells in Fig. 9 is wide enough that the free energy in the middle is reasonably constant. Assuming that the constant represents the binding free energy of a dimer on the free terrace, the numerical value of the free energy, in Fig. 9(d), is shown relative to the value in the middle of each well. On this uniform scale, the dimer-wall interaction free energy can be easily evaluated. The dimer is bound to the left wall by $\sim 0.030 - 0.060$ eV. Furthermore, in the two data sets where the left wall is the SA side of an island (circles and squares), somewhat weaker binding (by half) is also evident in the position located two lattice sites from the wall, indicating both first and second nearest-neighbor attraction. This behavior is similar to that of the dimer next to the SA step (crosses). This similarity indicates that the origin of the additional binding is due to a local interaction with only the nearest dimer row of the step or island, although persisting to a distance of 2 lattice sites.

Whereas the interaction energy for a dimer at the side of an SA dimer row, whether at a step or at a single dimer wide island, is seemingly well defined, the interaction with other types of defects shows different behavior. For example, the left well wall in Fig. 9(c) is comprised of an unknown type of defect, and although the dimer binds to the defect with about the same interaction energy as to a step (shown by diamonds), the binding is only effective at the site right next to the defect. The free energy falls off to the free-terrace value already at the second nearest-neighbor site. Different binding configurations are also observed in the interactions of the dimer with the various walls on the right side of the wells, from no detectable free-energy difference at the coupled dimer (circles), to a strong repulsive interaction at the upper side of the SB step (squares).

At this time, a detailed physical understanding of the origin of the free energy differences of dimers near steps and defects is lacking. Whether local surface strain effects or electronic-structure bonding differences predominate is unknown. In fact, little is even known about the specific configurational structure of many of the sorts of defects typically found on this surface. Additional, more detailed experiments of the type presented in this work, combined with theoretical calculations, may lead to a better understanding of the exact nature of adsorbate interactions as well as providing insight into the detailed structure of the various defect configurations. As demonstrated by imaging the preferred binding site for monomers at steps and islands, observations of the relative stability and energetics of various atomic

configurations are necessary to enable the comparison and potential refinement of theoretical calculations.

Learning about the kinetics of monomer adsorption at steps, and the diffusion and interaction of dimers with steps and islands, is an important first step in understanding the propagation of the crystal lattice during growth. Future work will elucidate the additional details of the formation of the stable 4-atom units demanded by the surface reconstruction, *i.e.*, the formation and lifetime of metastable dimers and their subsequent capture of an additional 2 atoms.

I am grateful for many useful discussions with G. L. Kellogg, J. E. Houston, and P. J. Feibelman. This work performed at Sandia National Laboratories is supported by the U. S. Department of Energy under contract DE-AC04-94AL85000.

References:

- [1] J. D. Chadi, Phys. Rev. Lett., **59**, 1691 (1987).
- [2] Y. W. Mo and M. G. Lagally, Surf. Sci. **248**, 313 (1991).
- [3] Y. W. Mo, B. S. Swartzentruber, R. Kariotis, M. B. Webb, and M. G. Lagally, Phys. Rev. Lett. **63**, 2393 (1989). Y. W. Mo, R. Kariotis, B. S. Swartzentruber, M. B. Webb, and M. G. Lagally, J. Vac. Sci. Technol. A **8**, 201 (1990). Y. W. Mo, J. Kleiner, M. B. Webb, and M. G. Lagally, Phys. Rev. Lett. **66**, 1998 (1990).
- [4] Y. W. Mo, Ph.D. Thesis, University of Wisconsin-Madison, (1991).
- [5] Y. W. Mo, J. Kleiner, M. B. Webb, and M. G. Lagally, Surf. Sci. **268**, 275 (1992).
- [6] B. S. Swartzentruber, Y. W. Mo, M. B. Webb, and M. G. Lagally, Phys. Rev. Lett. **65**, 1913 (1990).
- [7] H. J. W. Zandvliet, H. B. Elswijk, E. J. van Loenen, and D. Dijkkamp, Phys. Rev. B **45**, 5965 (1992).
- [8] B. S. Swartzentruber, N. Kitamura, R. Kariotis, M. G. Lagally, and M. B. Webb, Phys. Rev. B **47**, 13432 (1993).
- [9] H. J. W. Zandvliet, H. B. Elswijk, and E. J. van Loenen, Surf. Sci. **272**, 264 (1992).
- [10] N. Kitamura, B. S. Swartzentruber, M. G. Lagally, and M. B. Webb, Phys. Rev. B **48**, 5704 (1993).
- [11] B. S. Swartzentruber and M. Schacht, Surf. Sci. **322**, 83 (1995).
- [12] C. Pearson, B. Borovsky, M. Krueger, R. Curtis, and E. Ganz, Phys. Rev. Lett. **74**, 2710 (1995).
- [13] D. Dijkkamp, E. J. van Loenen, and H. B. Elswijk, in *Ordering at Surfaces and Interfaces*, edited by A. Yoshimori, T. Shinjo, and H. Watanabe (Springer-Verlag, Berlin, Heidelberg, 1992), p. 85.
- [14] B. S. Swartzentruber, Phys. Rev. Lett. **76**, 459 (1996).
- [15] Z. Zhang, F. Wu, H. J. W. Zandvliet, B. Poelsema, H. Metiu, and M. G. Lagally, Phys. Rev. Lett. **74**, 3644 (1995).
- [16] P. Bedrossian, Phys. Rev. Lett. **74**, 3648 (1995).
- [17] B. S. Swartzentruber, A. P. Smith, and H. Jónsson, Phys. Rev. Lett. **77**, 2518 (1996).

- [18] R. A. Wolkow, Phys. Rev. Lett. **74**, 4448 (1995).
- [19] F. Wu, Ph.D. Thesis, University of Wisconsin-Madison, (1996).
- [20] for a recent comprehensive review see Feng Liu and M. G. Lagally, in *The Chemical Physics of Solid Surfaces and Heterogeneous Catalysis*, edited by D. A. King and D. P. Woodruff (Elsevier Science Publishers, Amsterdam, 1996), (in press).
- [21] G. Brocks, P. J. Kelly, and R. Car, Phys. Rev. Lett. **66**, 1729 (1991).
- [22] Jun Wang, D. A. Drabold, and A. Rockett, Appl. Phys. Lett. **66**, 1954 (1995).
- [23] Jun Wang, D. A. Drabold, and A. Rockett, Surf. Sci. **344**, 251 (1995).
- [24] Q.-M. Zhang, C. Roland, P. Boguslawski, and J. Bernholc, Phys. Rev. Lett. **75**, 101 (1995).
- [25] C. Roland and G. H. Gilmer, Phys. Rev. Lett. **67**, 3188 (1991); Phys. Rev. B **46**, 13437 (1992).
- [26] Z. Y. Zhang, Y. T. Lu, and H. Metiu, Phys. Rev. B **46**, 1917 (1992).
- [27] D. Srivastava and B. J. Garrison, Phys. Rev. B **47**, 4464 (1993).
- [28] B. S. Swartzentruber, Y. W. Mo, M. B. Webb, and M. G. Lagally, J. Vac. Sci. Technol. A **8**, 210 (1990).
- [29] see for example, *Scanning Tunneling Microscopy*, eds. J. A. Stroscio and W. J. Kaiser (Academic Press, Inc. 1993).
- [30] R. J. Hamers, R. M. Tromp, and J. E. Demuth, Surf. Sci. **181**, 346 (1987).
- [31] G. Brocks and P. J. Kelly, Phys. Rev. Lett. **76**, 2362 (1996).
- [32] G. L. Kellogg, Surf. Sci. Reports **21**, 1 (1994).

Figure Captions:

Fig. 1. Schematic of Si(001) surface showing various step terminations. Normal (rebonded) substrate dimer bonds are shown in black (gray). Two monomers, "M", are depicted bound to trap sites at rebonded positions.

Fig. 2. Filled a), c) and empty b), d) state images of sub-monolayer Si growth on Si(001). Each pair of images, a)-b) and c)-d), were acquired simultaneously at room temperature. A single-dimer-wide island is indicated by the arrows.

Fig. 3. Empty-state images of two pairs of monomer traps between which a monomer switches back and forth at 105 C. The traps are separated by 11 and 3 lattice sites in a) and b) respectively. Location of monomer indicated by arrows.

Fig. 4. A monomer (indicated by arrows) and nearest-neighbor traps at 105 C. a) Two traps comprised of short segments of neighboring dimer rows in an island. b) Section of SB step comprising a set of 4 aligned traps.

Fig. 5. ~ 125 Å, filled-state STM image of two Si dimers trapped in wells between an SA step and vacancy-type defects acquired at 110 C. The upper well contains 4 sites and the lower well contains 6 sites

Fig. 6. Atom-track data of the position (along the substrate dimer row) of a dimer versus time in the well with 4 sites between an SA step and vacancy-type defect acquired at 110 C. This data set contains 13000 points.

Fig. 7. Residence-time distribution plots for the 4-site well between step and vacancy-type defect at 110 C. (a) Measured residence-time distribution from all of the sites (circles). Dashed line shows exponential falloff with measured average residence time, and solid line is weighted sum of exponentials from individual sites. (b) Measured residence-time distributions at each site.

Fig. 8. Relative free energy versus distance from the step in the 4 (circles) and 6 site (squares) wells between the step and vacancy-type defect. Values extracted from the relative occupation probabilities at 110 C.

Fig. 9. Data from dimers trapped in 3 different well configurations at 110C. (a)-(c) ~ 100 Å, empty-state images of wells containing: (a) 10, (b) 12, and (c) 14 sites. (d) Relative binding free energy as a function of distance from the left wall. Circles, squares, and diamonds are from wells shown in (a), (b), and (c) respectively. Crosses are data from the 6 site well at the bottom of Fig. 5. The statistical errors are on the scale of the symbol size.

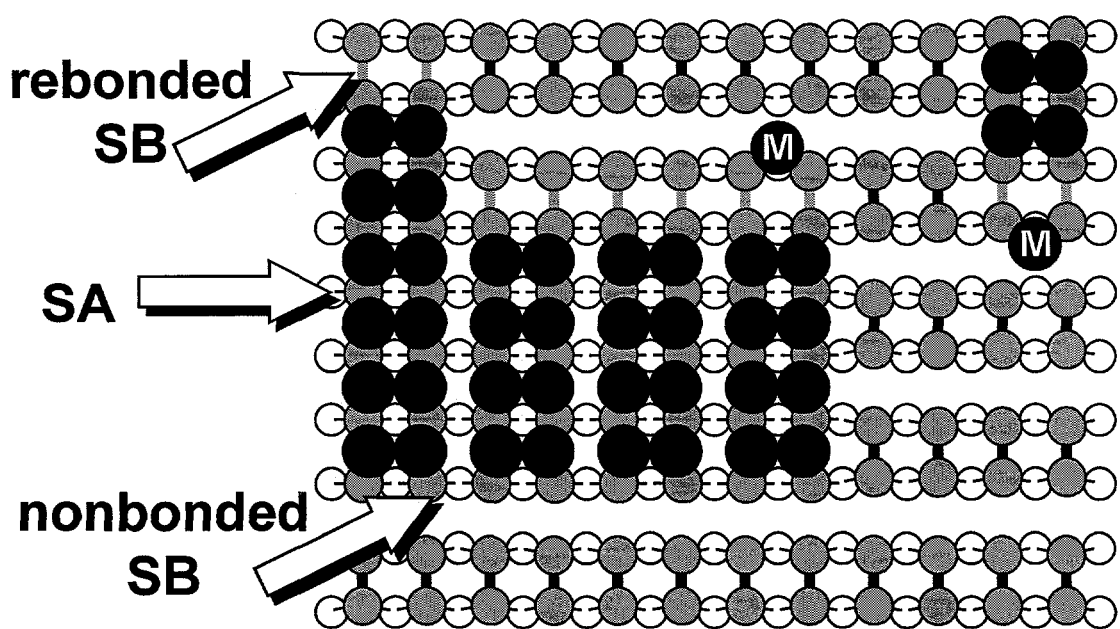


Fig. 1 Swartzentruber

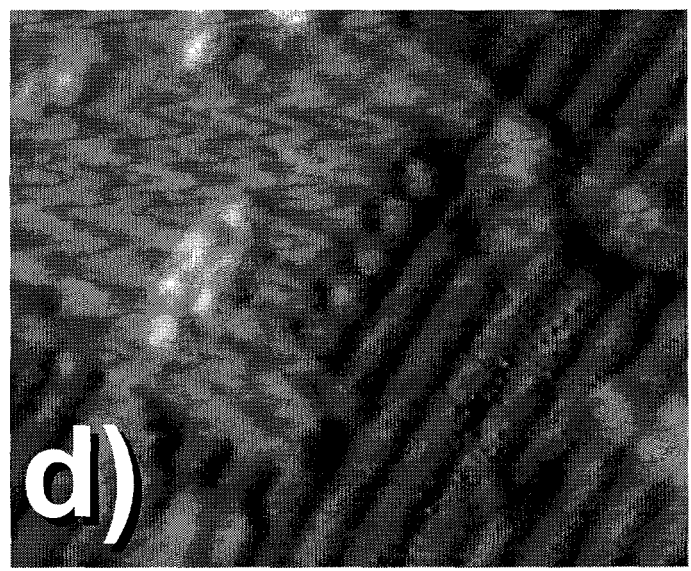
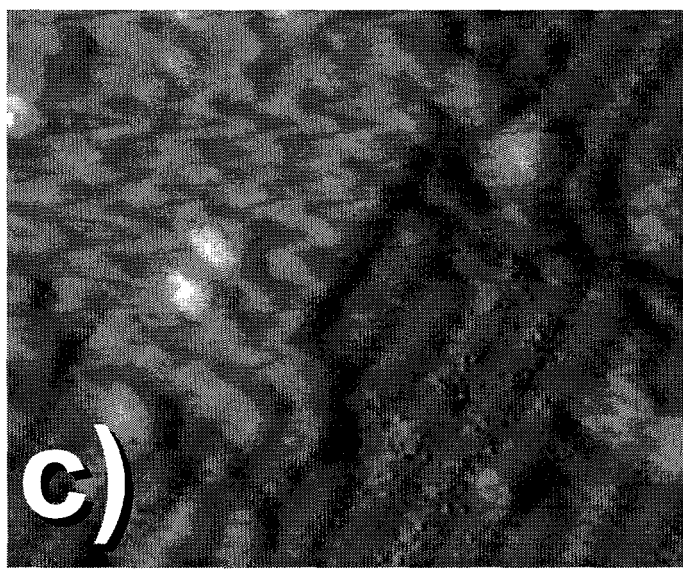
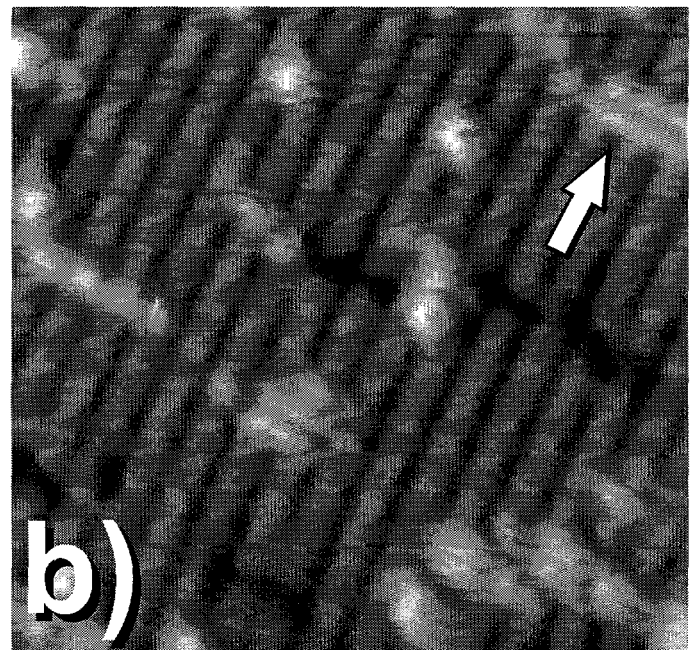
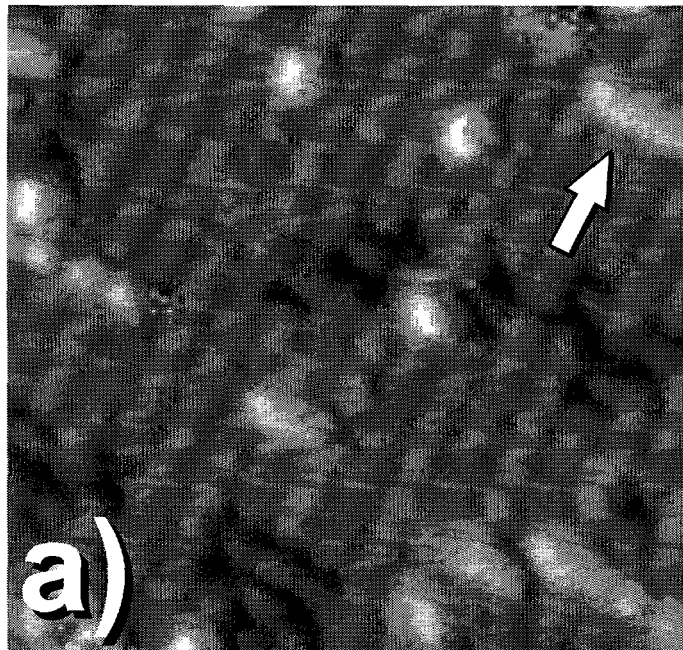


Fig. 2 Swartzentruber

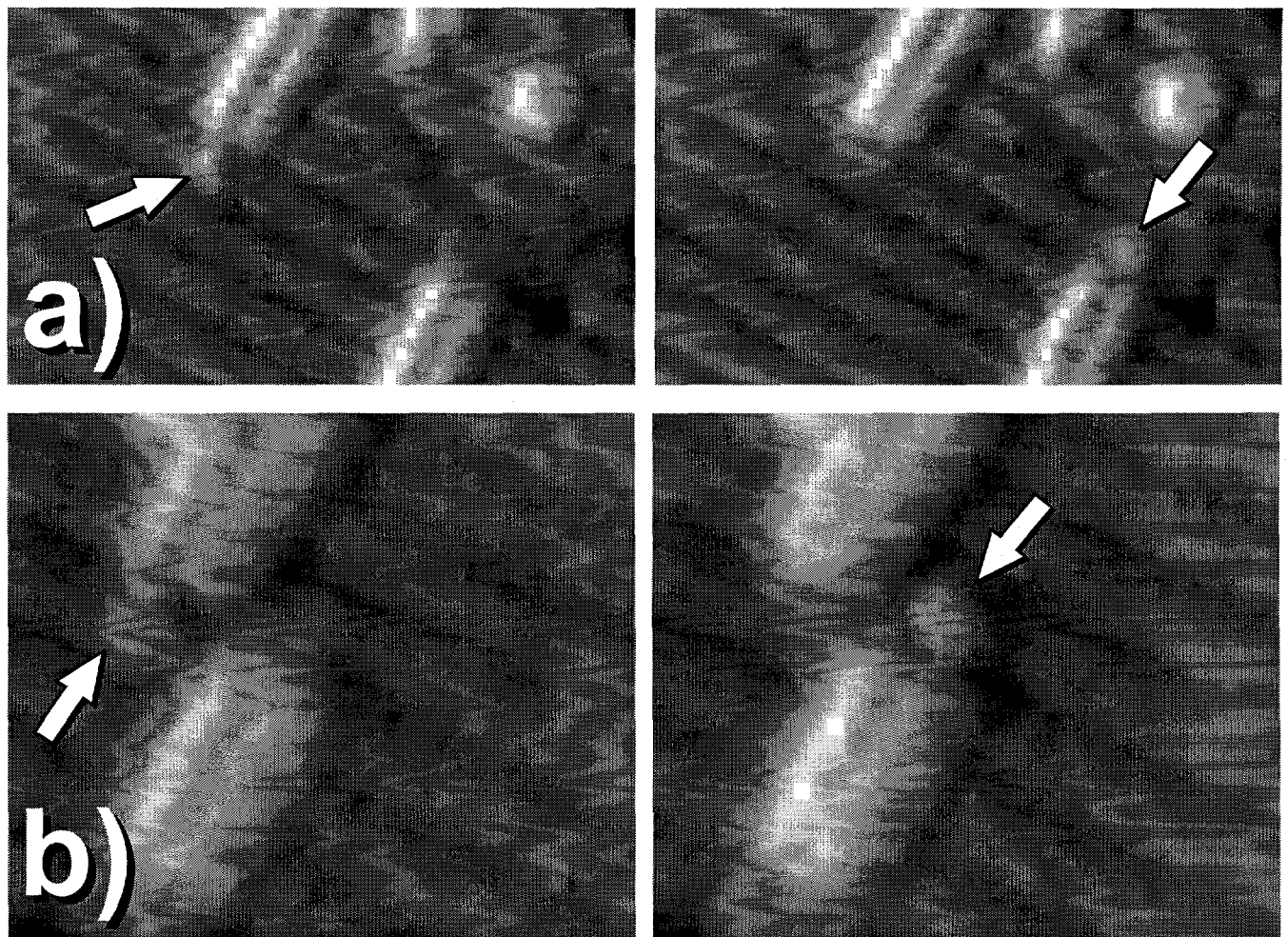


Fig. 3 Swartzentuber

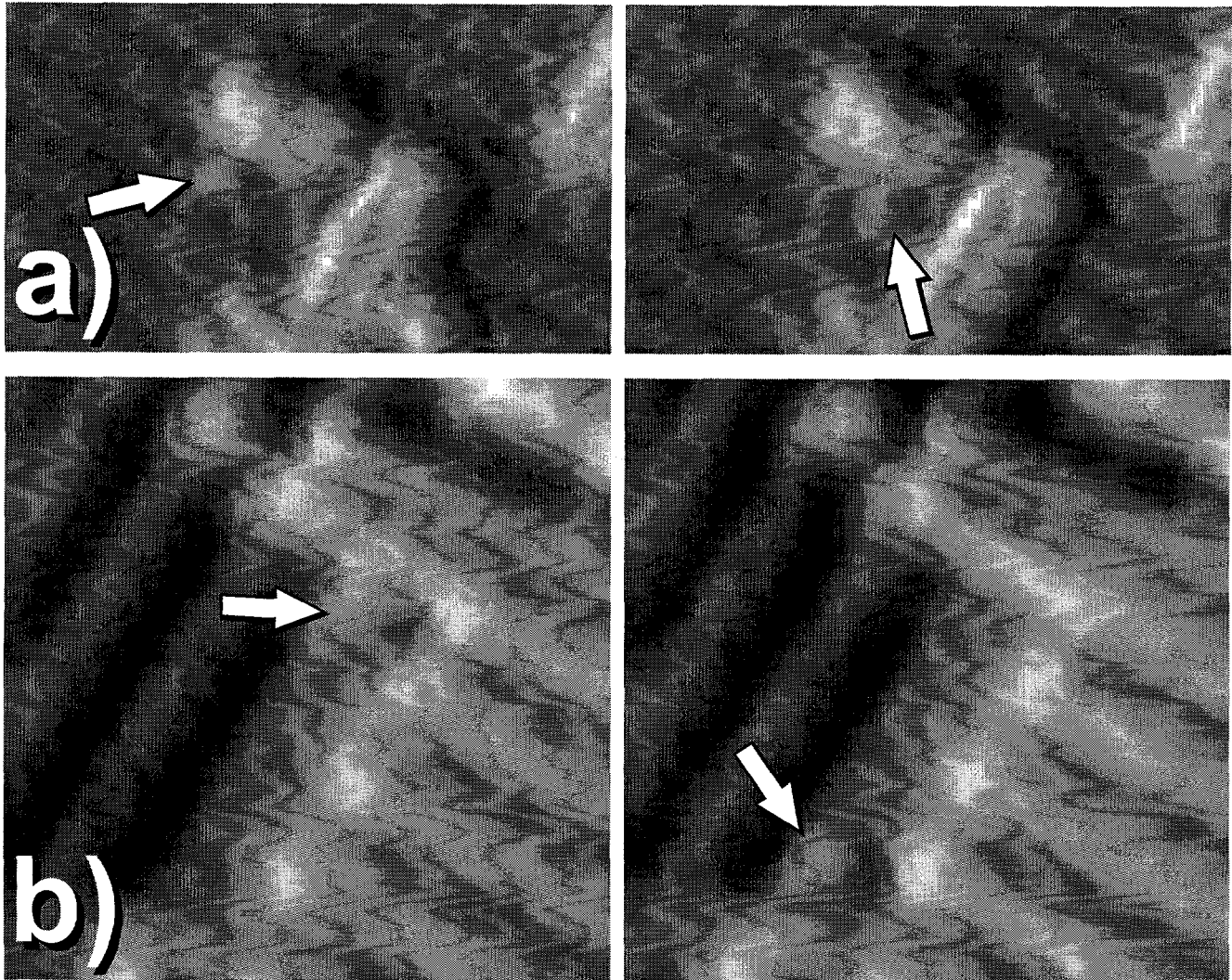


Fig. 4 Swartzentuber

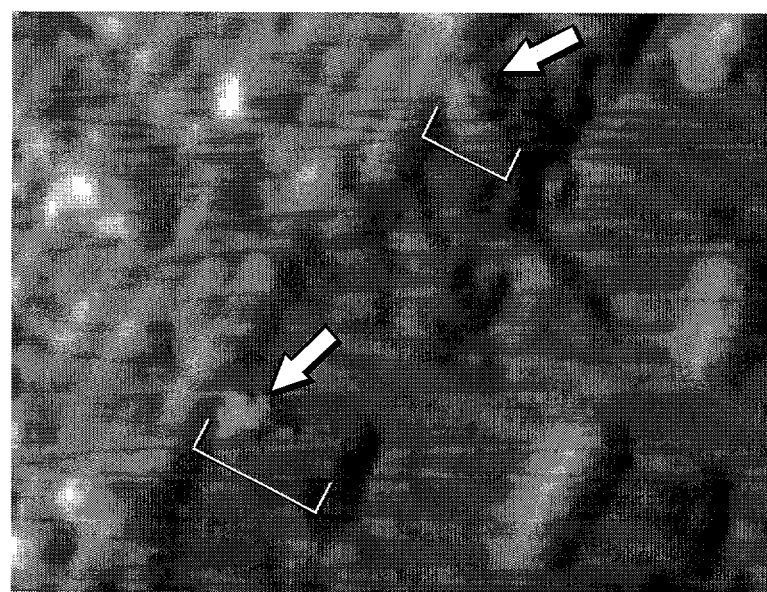


Fig. 5 Swartzentruber

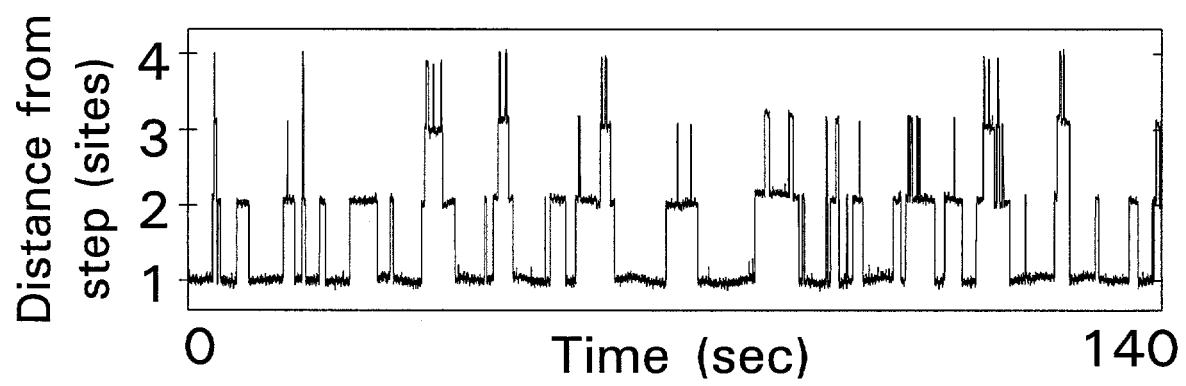


Fig. 6 Swartzentruber

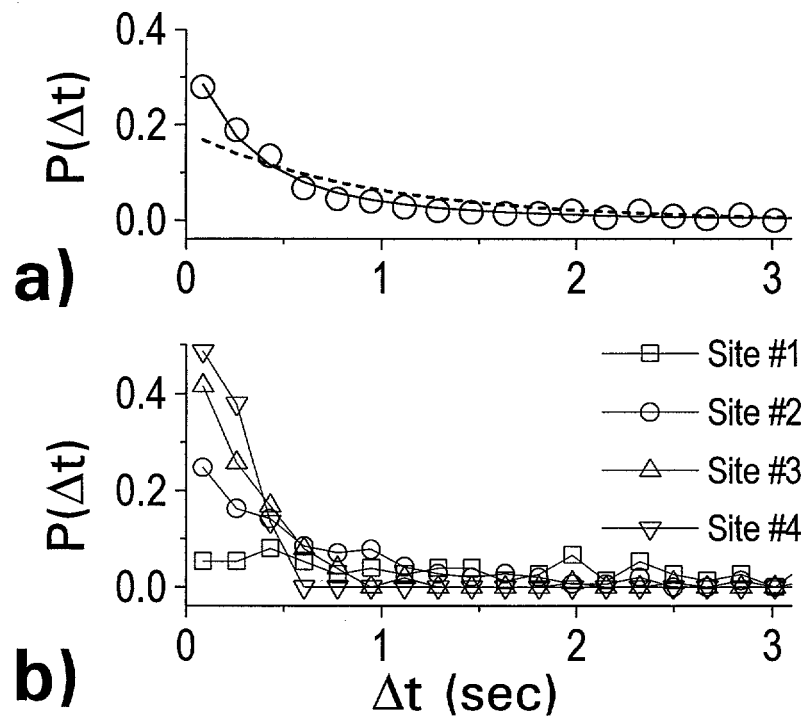


Fig. 7 Swartzentruber



Fig. 8 Swartzentruber

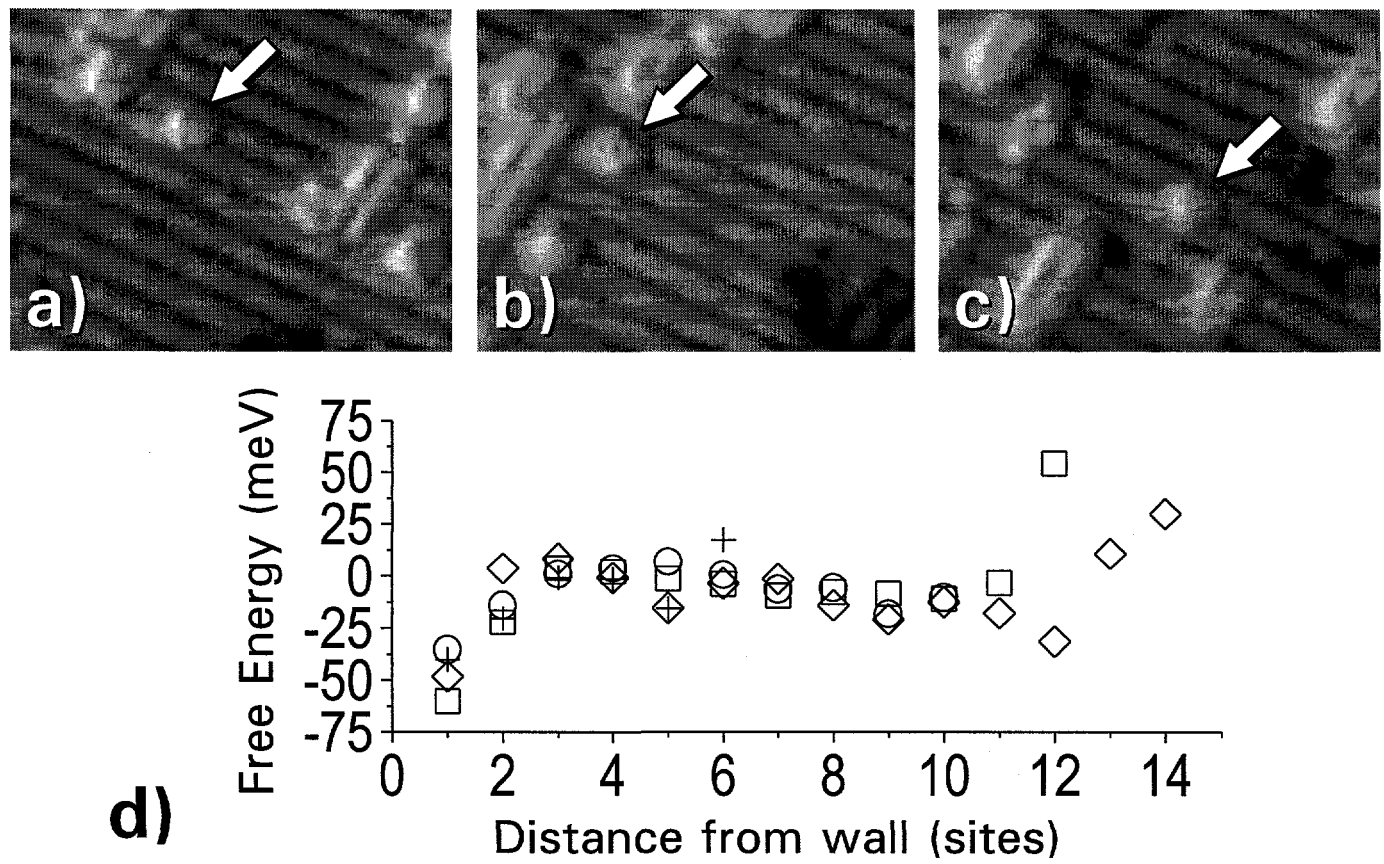


Fig. 9 Swartzentruber